Article:

Baas, JH, Best, J and Peakall, J orcid.org/0000-0003-3382-4578 (2021) Rapid gravity flow transformation revealed in a single climbing ripple. Geology, 49 (5). pp. 493-497. ISSN 0091-7613

https://doi.org/10.1130/G48181.1

Rapid gravity flow transformation revealed in a single climbing ripple

Jaco H. Baas[1], Jim Best[2] and Jeff Peakall[3]

[1]School of Ocean Sciences, Bangor University, Menai Bridge LL59 5AB, UK, e-mail: j.baas@bangor.ac.uk

[2]Departments of Geology, Geography and GIS, Mechanical Science and Engineering, and Ven Te Chow Hydrosystems Laboratory, University of Illinois at Urbana-Champaign, Urbana, IL 61801, USA

[3]School of Earth and Environment, University of Leeds, Leeds, LS2 9JT, UK

ABSTRACT

Sediment gravity flows possess a wide range of rheological behaviors and past work has shown how transformations between flow types generate spatiotemporal changes in the resultant sedimentary successions. Herein, the geometrical characteristics of a single climbing ripple are used to demonstrate how such flows can transform from a turbulent to a quasi-laminar plug flow, with the transitional clay flow sequence being manifested by abnormally large heterolithic sand–clay current ripples with small backflow ripples, and then abundant clay deposition associated with smaller ripples. Analysis of ripple size, angle of climb, grain size, internal erosional surfaces and soft-sediment deformation suggest that transformation in the rheological character of the sediment gravity flow was rapid, occurring over a period of tens of minutes, and thus probably over a spatial scale of hundreds of meters to several kilometers. The present study indicates how the character of flow transformation can be elucidated from the details of a small-scale sedimentary structure.

INTRODUCTION

Sediment gravity flows (SGFs) in oceans and lakes are a vital component of the global sediment cycle (Hessler and Fildani, 2019), and are equally important for the transport of organic carbon, nutrients and pollutants (e.g., plastics; Kane et al., 2020), pose a hazard to infrastructure (Clare et al., 2019), and their deposits may store hydrocarbons (Talling, 2014). The research and socio-economic relevance of SGFs is widely appreciated, but studying SGFs is challenging because of their unsteady and non-uniform behavior. This is exacerbated by the fact that most SGFs carry clay particles that aggregate to form floccules and gels, and thus enhance or suppress the shear-generated turbulence that helps drive these flows and shape their deposits (Baas et al., 2009; Baker et al., 2017). Detailed studies of SGF deposits have shown that these complex kinematics are expressed in the ability of SGFs to transform between turbulent, transitional and laminar behavior (Haughton et al., 2009), on which the concentration of suspended clay has a key influence (Baas et al., 2011). As clay concentration increases, these flow types comprise: (a) turbulence-enhanced transitional flow (TETF), in which turbulence is enhanced relative to clay-free turbulent flow; (b) lower transitional plug flow (LTPF), in which near-bed enhanced turbulence exists below a moving plug with suppressed turbulence; (c) upper transitional plug flow (UTPF), which has a thickened plug flow zone above a thinned, near-bed, zone of attenuated turbulence; and (d) quasi-laminar plug flow (QLPF), in which the plug extends down to the bed and turbulence is weak to absent (Baas et al., 2009). The characteristic bedforms formed by transitional flow are large ripples in TETF and LTPF and low-amplitude bed-waves in UTPF and QLPF (Baas et al., 2016). Large ripples have greater heights and wavelengths than ripples formed in clearwater, and low-amplitude bed waves are significantly longer and flatter than ripples generated in turbulent flows (Baker and Baas, 2020). Herein, we provide evidence for progressive SGF transformation preserved in a single climbing ripple, which stores a continuous record of bed aggradation and bedform migration. Since climbing ripples can form rapidly, especially at steep angles of climb associated with rapid aggradation rates (Allen, 1963), our analysis implies that flow transformation can occur in several tens of minutes. This timescale may be typical of transforming SGFs in confined basins (e.g., Fonnesu et al., 2015), but it is considerably shorter than for SGFs transforming in unconfined basins, which are usually 10s to 100s of km long and last for several hours to days or even weeks (Azpiroz-Zabala et al., 2017).

MATERIAL AND METHODS

We investigated a climbing-ripple set in a polished slab from the Seathwaite Fell Sandstone Formation (Ordovician, Elterwater Quarry, UK, 54.435°N, 3.046°W). This set forms a representative part of a climbing ripple co-set with similar sedimentological properties (Fig. 1A; Supplementary Material; Fig. S1), formed by deposition from a volcaniclastic mixed sand–clay gravity flow in a caldera lake (Branney and Kokelaar, 1994). The Seathwaite Fell Sandstone Formation contains various other types of primary current lamination, and soft-sediment deformation structures, denoting high sediment accumulation rates and seismic instability (Barnes et al., 2006).

The climbing-ripple set was divided into three sectors, based on textural properties, and 21 ripple positions were defined in these sectors by tracing ripple outlines (Fig. 1B). These positions were then used to determine the evolution of ripple height (Fig. 1C; the vertical distance between ripple trough and crest), and, where possible, ripple wavelength (the horizontal distance between adjacent ripple troughs). Ripple brinkpoints were traced to determine changes in angle of climb, and the size of sand grains was measured using a Dino-Lite digital microscope. Ripple types were then interpreted, based on ripple size and their turbulent, transitional and laminar flow signatures (Baas et al., 2009, 2011, 2016). Finally, qualitative evidence for rapid bed aggradation was combined with quantitative analysis using several methods (Fig. 1D) that have been proposed previously (Supplementary Material; Ashley et al., 1982; Baas, 1993, 2004; Baas et al., 2000, 2009; Jobe et al., 2012) to determine bed aggradation rates (Supplementary Material) and estimate the duration of deposition of the climbing-ripple set.

THE CLIMBING-RIPPLE SET EXPLAINED KINEMATICALLY

Description: In Sector 1 (yellow lines, Fig. 1B), the ripple is sandy and climbs over a vertical distance of 15.6 mm at a mean angle of 19.7°. Sector 2 is 27.7 mm thick, with a mean angle of climb of 18.4° (orange lines, Fig. 1B), and possesses distinct foreset laminae of alternating sand and clay. The mean sand size in Sectors 1 and 2 is 0.124 mm. Sector 3 (red lines, Fig. 1B) is clay-rich with occasional thin, discontinuous, silty laminae; the ripple climbs over a vertical distance of 21.6 mm at a mean angle of 44.2°. The ripple height in Sector 1 increases from 8.5 to 12.9 mm (Figs. 1C and 2), and keeps growing in Sector 2, until it reaches a maximum height of 21.7 mm at the transition to Sector 3 (Figs 1C and 2). In Sector 3, ripple height and wavelength decrease from 21.7 to 18.4 mm (Figs 1C and 2) and from 174 to 183 mm (Fig. 1B), respectively.

Interpretation: The final ripple height of 12.9 mm in Sector 1 is less than 14.9 mm, the height at which equilibrium ripples form in 0.124 mm sand under clearwater flow (Baas, 1993; Fig. 2). It is therefore inferred that this ripple did not reach equilibrium and evolved between non-equilibrium heights of 8.5 and 12.9 mm. The sandy nature of Sector 1 suggests that any suspended clay present did not affect the flow kinematics or become incorporated into the bed. Hence, this ripple formed in a 'classic' fully turbulent flow (Baas et al., 2011; Fig. 3B). The ripple grew in height throughout Sector 2 (Figs. 2 and 3C), with the final height of 21.7 mm matching the so-called 'large ripples' generated in the laboratory (Baas et al., 2016) and described in outcrop (Baker and Baas, 2020; Fig. 2). Large ripples form in TETF and LTPF (Baas et al., 2011; Fig. 3C), in which enhanced turbulence in ripple troughs (Baas and Best, 2008) helps to increase ripple size. This turbulence enhancement requires a local increase in suspended clay concentration, possibly combined with flow deceleration (Figs 3C and S2). Further support for TETF and LTPF comes from: (a) alternating sandy and clayey laminae in Sector 2, which mimics large ripples in the laboratory (Baas et al., 2011, 2016); (b) small backflow ripples near the base of the ripple foreset (Fig. S3), pointing to strong vorticity and upstream flow velocities in the ripple trough (Baas et al., 2011); and (c) a finer-grained core (sensu Baker and Baas, 2020), especially in the top half of Sector 2 (Fig. 1A), across which the sandy part of the ripple migrated, signifying concurrent bedload transport of sand and fallout from suspension of clay. The ripple in Sector 3 has a smaller height than in Sector 2 (Fig. 2), interpreted as the product of a further increase in local suspended clay concentration combined with flow deceleration in an UTPF or QLPF (Supplementary Material) that caused the ripple height to decrease (Fig. 3D). This is supported by the high clay content in Sector 3, denoting significant fallout from suspension, and the fact that Baker and Baas (2020) have shown that such flows form low-amplitude bed-waves, the height of which is much smaller (mostly below 10 mm) and the wavelength of which is larger (200-800 mm) than for ripples in turbulent and turbulence-enhanced flows. However, the bedform in Sector 3 did not reach these heights and wavelengths (Fig. 2), probably because ripple development was temporarily constrained and the high suspended clay concentration hindered evolution from large ripples to low-amplitude bed-waves. These bedforms can therefore be classified as relict large ripples.

The ripple studied herein climbed at high mean angles of 18.4° to 44.2°, suggesting that the vertical aggradation rate became larger relative to the migration rate (Supplementary Material). Various quantitative methods (Fig. 1D; see Supplementary Material for details) show that a period of the order of tens of minutes, with extremes in the Sectors 1 to 3 of 1.2-38.8 minutes, 5.9-125 minutes, and 8.2-69 minutes, respectively, was sufficient to deposit the climbing-ripple set. Such rapid development is also supported by qualitative data (Fig. 1A): (a) Strong erosion (>10 mm deep, Figs 1A and 3A) and soft-sediment deformation of clay-rich sediment at the base of the climbing-ripple co-set indicate that the initial flow conditions were strong enough to deform and erode cohesive clay. The occasional presence of mud clasts confirms that the substrate was firm. (b) Flow in the ripple trough was fast enough to scour into the stoss side of the downstream ripple in Sectors 1 and 2 (Fig. 1A). (c) soft-sediment deformation in Sector 3 (Fig. 1A) may indicate water-rich sediment linked to rapid deposition (Barnes et al., 2006). This deformation was synsedimentary because local deformation is healed by younger laminae.

FLOW TRANSFORMATION IN CLIMBING RIPPLES: IMPLICATIONS

The present study reveals that climbing ripples can preserve continuous records of transformation from turbulent via transitional to laminar flow in a waning, mixed sand–clay, gravity current (Fig. 3), and it confirms that kinematic process models for ripples in sand do not apply to ripples in mixed sand–clay (Baas et al., 2016; Baker and Baas, 2020). This is not unique to the Seathwaite Fell Sandstone Formation. Climbing-ripple co-sets with an upward increase in angle of climb, and wavelength, are one of three climbing ripple patterns in the classification of Allen (1973), and have been linked to ‘collapsing flows’ in SGFs (Jobe et al., 2012), implying that suspension fallout rates increased during deposition relative to bedload transport rate. However, this does not explain the simultaneous increase in ripple wavelength. We infer that the steep angle of climb near the top of co-sets is caused not only by a strong increase in suspension fallout rate (e.g., Sorby, 1908; Allen, 1963; Hunter, 1977) and a decrease in ripple migration rate at decreased flow velocity (cf., Jopling and Walker, 1968), but also by a slowing of ripple migration through turbulence attenuation induced by cohesive clay (Baas et al., 2011). The mud-rich, longer-wavelength bedforms similar to those in Sector 3, found at the top of these sequences (Walker, 1963; Jopling and Walker, 1968; Bhattacherjee, 1970) also reflect flow transformation. For example, Bhattacherjee (1970) described muddy bedforms in the Cloridorme Formation (Québec, Canada), 13.6 mm high and 353 mm long, which match the size of low-amplitude bed-waves (Baas et al., 2016; Baker and Baas, 2020; Fig. 2). Bhattacherjee (1970) also described ripples with a similar wavelength but a larger height (27 mm; his figure 8) in clay-rich sandstones below climbing low-amplitude bed-waves, thus resembling large ripples (Baas et al., 2016; Baker and Baas, 2020; cf., Stanley, 1974; Fig. 2). This change from large ripples to low-amplitude bed-waves matches the climbing-ripple co-set studied herein, except that the bedforms in the Cloridorme Formation were able to fully complete this change.

It thus appears that the climbing ripples described herein are a common sedimentary structure. They resemble the Type-3 climbing ripple co-sets of Walker (1963; his table II), almost exclusively found in turbidites. Therefore, in addition to providing evidence for flow transformation, the mixed sand–clay climbing ripple co-sets described herein may also be a strong indicator for waning gravity flows in deep-marine or lacustrine depositional environments. In most scenarios, waning mixed sand–clay gravity flows must pass through flow types in which turbulence is first enhanced and then attenuated (Fig. S1), and thus large ripples and low-amplitude bed-waves can be expected to be common bedform types in mixed sand–clay climbing ripple co-sets. Together with sandy ripples, these bedforms provide a novel tool to reconstruct temporal changes in SGF kinematics.

The present analysis illustrates that rates of flow transformation in SGFs, and thus rates at which cohesivity may develop, can be as rapid as several tens of minutes. In the example described herein, this duration converts into flow lengths of hundreds of meters to several kilometers for flow velocities at which current ripples are stable. These temporal and spatial scales correspond to those inferred from the deposits of SGFs that comprise a hybrid between turbulent and laminar behavior in confined basins (e.g., Fonnesu et al., 2015). However, these scales are at least an order of magnitude shorter than for unconfined basins, which usually contain rapid flows that are 10s to 100s of km long (e.g., Haughton et al., 2009; Talling, 2013; Talling et al., 2013) and may last for several hours to days or even weeks (Azpiroz-Zabala et al., 2017). The present analysis shows that once such flows start to decelerate, transformation can occur rapidly, and that SGF deposits can leave evidence of this flow transformation at a scale of 10s of mm that can be recognized in cores and small outcrops.

CONCLUSIONS

The rate of flow transformation within a SGF is revealed by analysis of bedform size, grain size and the microstructure of cross-stratification within a single climbing ripple set. The present study demonstrates that an initially turbulent flow that is aggradational and generates climbing ripples, begins to develop large ripples in TETF or LTPF, as the flow decelerates. These large ripples are generated by increased turbulence in the ripple trough that causes additional scour that may also form small backflow ripples. These large ripples are also characterized by heterolithic deposition on the ripple leeside, as fallout from suspension becomes more dominant than sand and silt avalanching down the leeside slope. Further flow deceleration, and increases in clay concentration, cause more rapid aggradation, and higher angles of climb, of the clay-rich current ripple, which also becomes smaller due to the dampening of turbulence in UTPF or QLPF. Further analysis reveals that such flow transformation, from turbulent to quasi-laminar plug flow, was rapid and occurred over a period of tens of minutes, suggesting that the spatial distance over which such transformation took place was hundreds of meters to several kilometers. Quantification of the microstructure of such climbing ripple sequences may hold untapped potential for reconstructing the temporal fluid dynamics of clay-laden SGFs in many sedimentary environments.

ACKNOWLEDGMENTS

We thank Fiona Cameron, Burlington Stone, UK, for arranging access to these materials, and Zane Jobe, Matthieu Cartigny, and Bill Arnott for their insightful reviews.

REFERENCES CITED

Allen, J. R. L., 1963, Asymmetrical ripple marks and the origin of water-laid cosets of cross-strata: Liverpool Manchester Geological Journal, v. 3, p. 187-236.

Allen, J. R. L., 1973, A classification of climbing-ripple cross-lamination: Journal of the Geological Society of London, v. 129, p. 537-541.

Ashley, G. M., Southard, J. B., and Boothroyd, J. C., 1982, Deposition of climbing-ripple beds: a flume simulation: Sedimentology, v. 29, p. 67-79.

Azpiroz-Zabala, M., Cartigny, M. J. B., Talling, P. J., Parsons, D. R., Sumner, E. J., Clare, M. A., Simmons, S. M., Cooper, C., and Pope, E. L., 2017, Newly recognized turbidity current structure can explain prolonged flushing of submarine canyons: Science Advances, v. 3, e1700200.

Baas, J. H., 1993, Dimensional analysis of current ripples in recent and ancient depositional environments: Geologica Ultraiectina, v. 106, p. 199.

Baas, J. H., 2004, Conditions for formation of massive turbiditic sandstones by primary depositional processes: Sedimentary Geology, v. 166, p. 293-310.

Baas, J. H., and Best, J. L., 2008, The dynamics of turbulent, transitional and laminar clay-laden flow over a fixed current ripple: Sedimentology, v. 55, p. 635-666.

Baas, J. H., Best, J. L., Peakall, J., and Wang, M., 2009, A phase diagram for turbulent, transitional, and laminar clay suspension flows: Journal of Sedimentary Research, v. 79, p. 162-183.

Baas, J. H., Best, J. L., and Peakall, J., 2011, Depositional processes, bedform development and hybrid flows in rapidly decelerated cohesive (mud-sand) sediment flows: Sedimentology, v. 58, p. 1953-1987.

Baas, J. H., Best, J. L., and Peakall, J., 2016, Predicting bedforms and primary current stratification in cohesive mixtures of mud and sand: Journal of the Geological Society, v. 173, p. 12-45.

Baas, J. H., van Dam, R. L., and Storms, J. E. A., 2000, Duration of deposition from decelerating high-density turbidity currents: Sedimentary Geology, v. 136, p. 71-88.

Baker, M. L., and Baas, J.H., 2020, Mixed sand–mud bedforms produced by transient turbulent flows in the fringe of submarine fans: Indicators of flow transformation: Sedimentology, v. 67, p. 2645-2671.

Baker, M. L., Baas, J. H., Malarkey, J., Silva Jacinto, R., Craig, M. J., Kane, I. A., and Barker, S., 2017, The effect of clay type on the properties of cohesive sediment gravity flows and their deposits: Journal of Sedimentary Research, v. 87, p. 1176-1195.

Barnes, R. P., Branney, M. J., Stone, P., and Woodcock, N.H., 2006, The Lakesman Terrane: the Lower Palaeozoic record of the deep marine Lakesman Basin, a volcanic arc and foreland basin, *in* Brenchley, P.J., and Rawson, P.F., eds., The Geology of England and Wales, Geological Society, London, Geology Of Series, p. 103-130.

Bhattacharjee, S. B., 1970, Ripple-drift cross-lamination in turbidites of the Ordovician Cloridorme Formation, Gaspé, Québec [M.Sc. Thesis], McMaster University, Hamilton, Ontario, Canada, 281 p.

Branney, M. J., and Kokelaar, P., 1994, Volcanotectonic faulting, soft-state deformation, and rheomorphism of tuffs during development of a piecemeal caldera, English Lake District: Geological Society of America Bulletin, v. 106, p. 507-530.

Clare, M., Chaytor, J., Dabson, O., Gamboa, D., Georgiopoulou, A., Eady, H., Hunt, J., Jackson, C., Katz, O., Krastel, S., León, R., Micallef, A., Moernaut, J., Moriconi, R., Moscardelli, L., Mueller, C., Normandeau, A., Patacci, M., Steventon, M., Urlaub, M., Völker, D., Wood, L., and Jobe, Z., 2019, A consistent global approach for the morphometric characterization of subaqueous landslides: Geological Society, London, Special Publications, v. 477, p. 455-477.

Fonnesu, M., Haughton, P., Felletti, F., and McCaffrey, W., 2015, Short length-scale variability of hybrid event beds and its applied significance: Marine and Petroleum Geology, v. 67, p. 583-603.

Haughton, P., Davis, C., McCaffrey, W., and Barker, S., 2009, Hybrid sediment gravity flow deposits - Classification, origin and significance: Marine and Petroleum Geology, v. 26, p. 1900-1918.

Hessler, A.M., and Fildani, A., 2019, Deep-sea fans: Tapping into Earth's changing landscapes: Journal of Sedimentary Research, v. 89, p. 1171-1179.

Hunter, R.E., 1977, Terminology of cross-stratified sedimentary layers and climbing-ripple structures: Journal of Sedimentary Petrology, v. 47, p. 697-706.

Jobe, Z. R., Lowe, D. R., and Morris, W. R., 2012, Climbing-ripple successions in turbidite systems: depositional environments, sedimentation rates and accumulation times: Sedimentology, v. 59, p. 867-898.

Jopling, A. V., and Walker, R. G., 1968, Morphology and origin of ripple-drift cross-lamination, with examples from the Pleistocene of Massachusetts: Journal of Sedimentary Petrology, v. 38, p. 971-984.

Kane, I. A., Clare, M. A., Miramontes, E., Wogelius, R., Rothwell, J.J., Garreau, P., and Pohl, F., 2020, Seafloor microplastic hotspots controlled by deep-sea circulation: Science, v. 368, p. 1140-1145.

Sorby, H. C., 1908, On the application of quantitative methods to the study of the structure and history of rocks: Quarterly Journal of the Geological Society of London, v. 64, p. 171-233.

Stanley, K. O., 1974, Morphology and hydraulic significance of climbing ripples with superimposed micro-ripple-drift cross-lamination in lower Quaternary lake silts, Nebraska: Journal of Sedimentary Petrology, v. 44, p. 472-483.

Talling, P. J., 2013, Hybrid submarine flows comprising turbidity current and cohesive debris flow: Deposits, theoretical and experimental analyses, and generalized models: Geosphere, v. 9, p. 460-488.

Talling, P. J., 2014, On the triggers, resulting flow types and frequencies of subaqueous sediment density flows in different settings: Marine Geology, v. 352, p. 155-182.

Talling, P. J., Paull, C. K., and Piper, D. J. W., 2013, How are subaqueous sediment density flows triggered, what is their internal structure and how does it evolve? Direct observations from monitoring of active flows: Earth-Science Reviews, v. 125, p. 244-287.

Walker, R. G., 1963, Distinctive types of ripple-drift cross-lamination: Sedimentology, v. 2, p. 173-188.

FIGURE CAPTIONS

Figure 1. (A) Climbing-ripple co-set in Seathwaite Fell Sandstone Formation, UK. Inset shows location of (B). Flow direction is towards right. (B) High-contrast image of the climbing-ripple set, highlighting 21 ripple outlines in Sectors 1 (yellow), 2 (orange), and 3 (red). Blue dashed line traces the ripple brinkpoints. Inset shows location of Fig. S3. TF = turbulent flow; TETF = turbulence-enhanced transitional plug flow; LTPF/UTPF = lower/upper transitional plug flow; QLPF = quasi-laminar plug flow. (C) Horizontal position of the ripple brinkpoint vs ripple height and angle of climb for the three sectors. Numbers refer to ripple outlines in (B). (D) Estimated durations of deposition of Sectors 1 (yellow), 2 (orange), and 3 (red), using the methods described in the Supplementary Material. Note that the range for bed sediment flux & ripple height in Sector 2 may be overestimated (see Supplementary Material).

Figure 2. Compilation of wavelengths and heights for sandy ripples, large ripples and low-amplitude bed-waves. Black box: predicted size range of non-equilibrium and equilibrium ripples in 0.124 mm sand (Baas, 1993). Yellow dots: sandy ripples for a range of grain sizes. Note that all large ripples and low-amplitude bed-waves are outside the size range of ripples in 0.124 mm sand.

Figure 3. Schematic model for the formation of the climbing-ripple set. (A) Erosion by turbulent flow front. (B) Sandy ripples formed by turbulent body of flow. (C) Mixed sand–clay large ripples formed by turbulence-enhanced flow. (D) Clay-rich ripples formed by turbulence-attenuated flow. (E) Schematic temporal changes in flow velocity, near-bed clay concentration and turbulence, sand and clay aggradation rate, and angle of climb. See Fig. 1 for explanation of flow types.

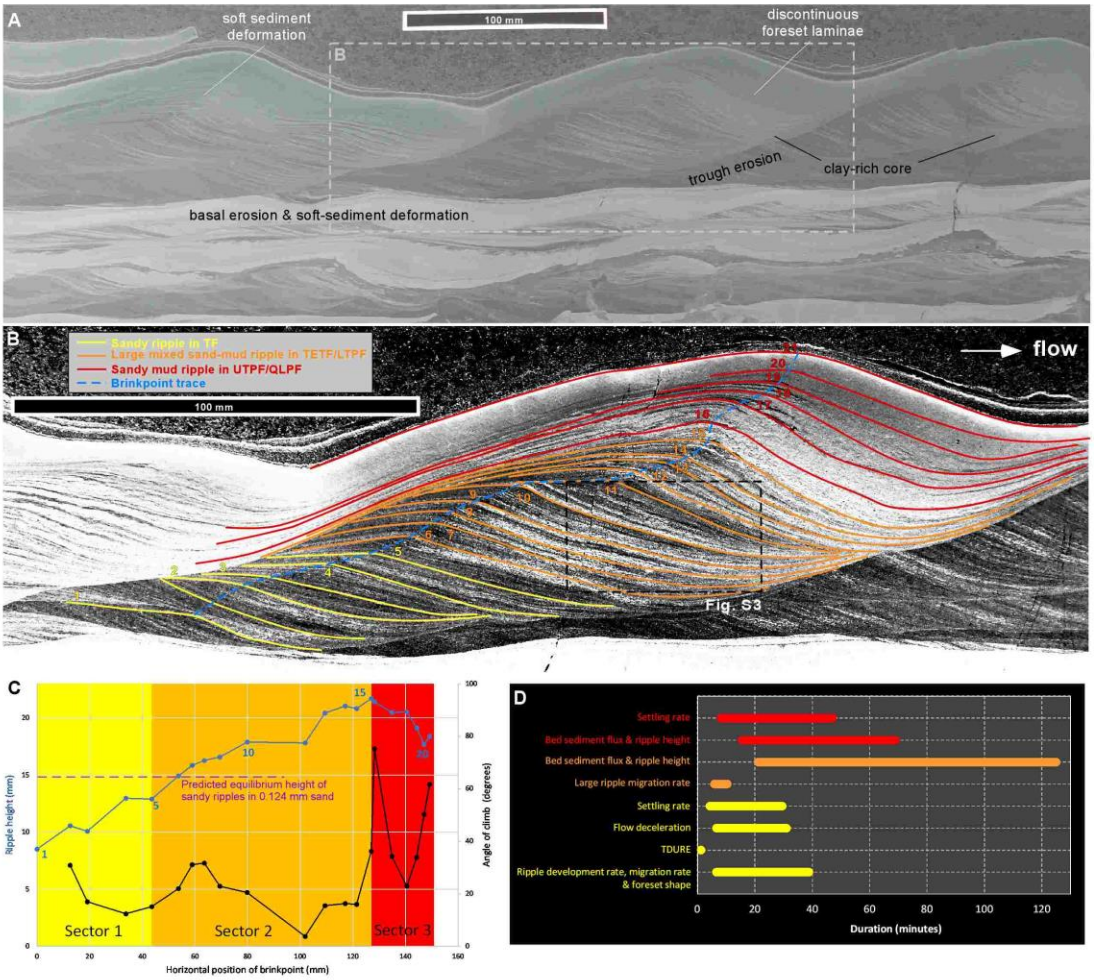
A
soft sediment deformation
100 mm
discontinuous foreset laminae
B
trough erosion
clay-rich core
basal erosion & soft-sediment deformation
B
Sandy ripple in TF
Large mixed sand-mud ripple in TETF/LTPF
Sandy mud ripple in UTPF/QLPF
Brinkpoint trace
flow
100 mm
Fig. S3
C
Ripple height (mm)
Angle of climb (degrees)
Predicted equilibrium height of sandy ripples in 0.124 mm sand
Sector 1
Sector 2
Sector 3
Horizontal position of brinkpoint (mm)
D
Settling rate
Bed sediment flux & ripple height
Bed sediment flux & ripple height
Large ripple migration rate
Settling rate
Flow deceleration
TDURE
Ripple development rate, migration rate & foreset shape
Duration (minutes)

Figure 1

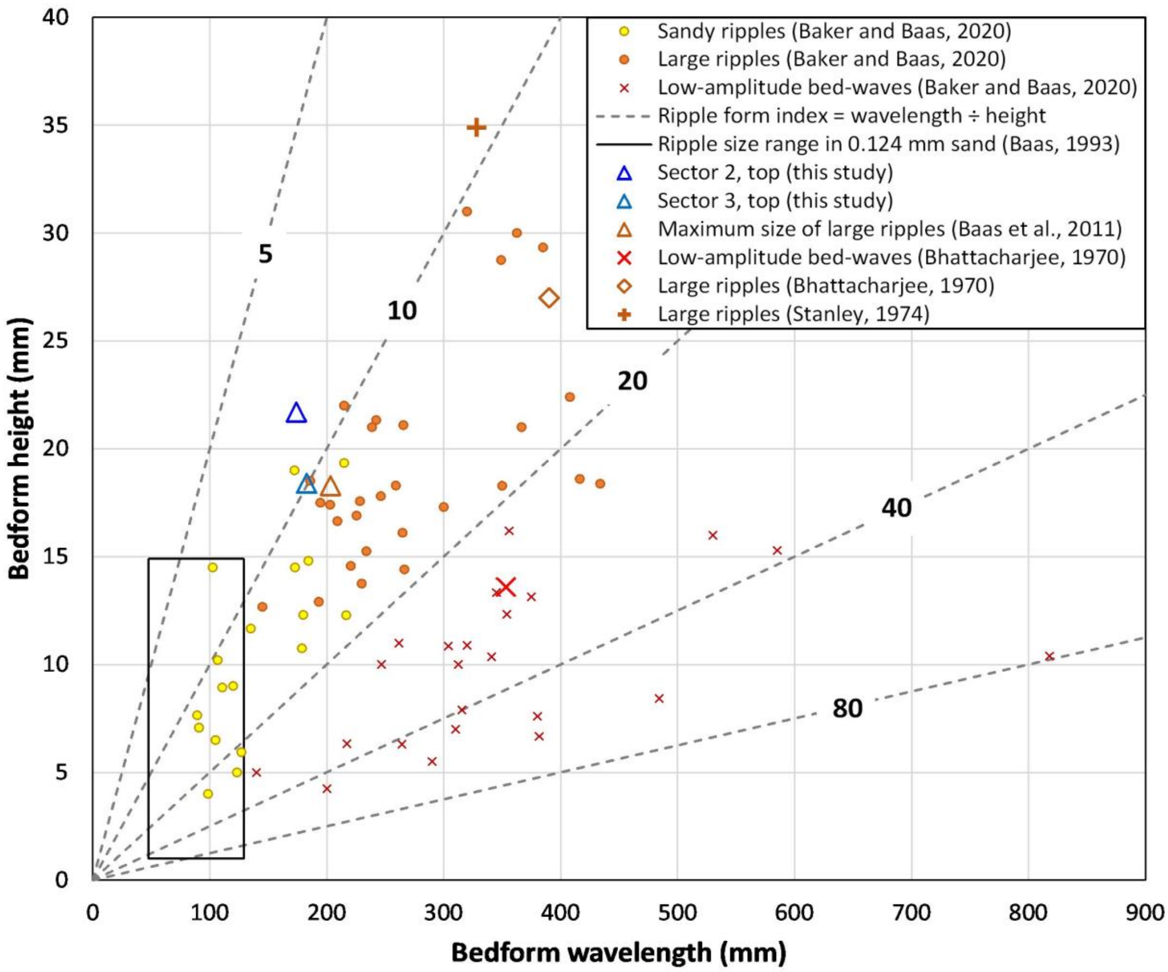

Sandy ripples (Baker and Baas, 2020)
Large ripples (Baker and Baas, 2020)
Low-amplitude bed-waves (Baker and Baas, 2020)
Ripple form index = wavelength ÷ height
Ripple size range in 0.124 mm sand (Baas, 1993)
Sector 2, top (this study)
Sector 3, top (this study)
Maximum size of large ripples (Baas et al., 2011)
Low-amplitude bed-waves (Bhattacharjee, 1970)
Large ripples (Bhattacharjee, 1970)
Large ripples (Stanley, 1974)
5
10
20
40
80
Bedform height (mm)
Bedform wavelength (mm)
0
5
10
15
20
25
30
35
40
0
100
200
300
400
500
600
700
800
900

Figure 2

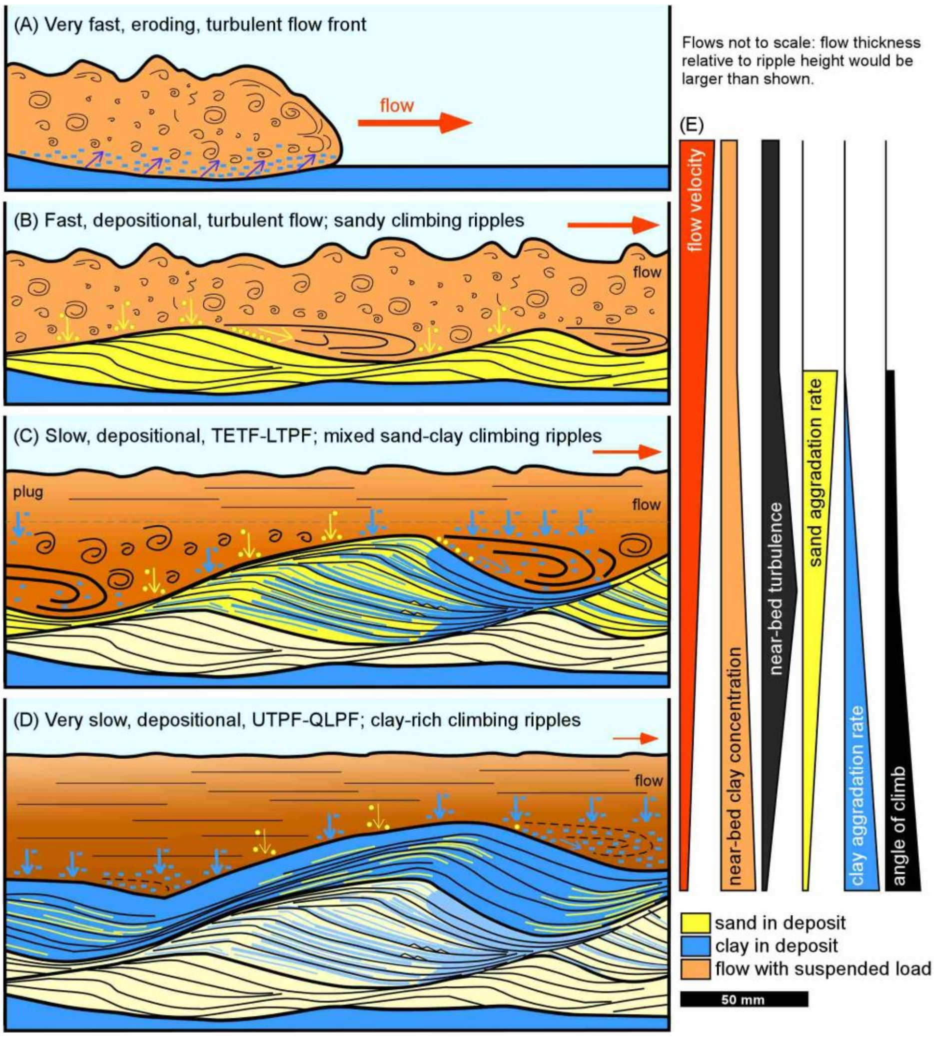

305

306 Figure 3

COMPARISON OF CLIMBING-RIPPLE SETS

The evolution of the height of the climbing ripple set described in the main text, as well as the climbing ripple set immediately downstream (right-hand side of Fig. 1A), are compared in Fig. S1. For both ripple sets, the height increases from *c.* 8 mm to 22-23 mm and then decreases to 15-17 mm. This suggests that both ripple sets evolved from sandy ripples via large ripples to relict large ripples. Moreover, low-amplitude bed-waves did not form, likely because of time constraints on ripple development and high suspended clay concentrations hindered evolution from large ripples to low-amplitude bed-waves, as described in the main text. Figure S1 also reveals that the downstream climbing ripple set reached its maximum height over a shorter migration distance than the climbing ripple set described in the main text, but the steepest decrease in height occurred at a similar migration distance. This difference in the rate of development is inferred to result from the dynamic behavior of rippled beds; individual ripples affect the local flow field, which may either promote or hinder the migration rate and development rate of adjacent ripples (Baas, 1993). In this case, the climbing ripple set described in the main text may have promoted the development of large ripples in the climbing ripple set immediately downstream. Despite this difference in evolution, both climbing ripple sets are sufficiently similar to support the main conclusion that evidence for rapid flow transformation can be preserved in climbing ripple co-sets.

QUANTITATIVE EVIDENCE FOR RAPID AGGRADATION IN THE CLIMBING-RIPPLE SET

The angle of climb of climbing-ripple co-sets is controlled by the ratio of the suspended sediment fallout rate to the rate of downstream ripple migration. Although a steep angle of climb is more likely caused by a high aggradation rate (Sorby, 1859; Reineck, 1961; Allen, 1963; Walker, 1963; Jopling & Walker, 1968; Środoń, 1974; Banerjee, 1977; Jobe et al., 2012), Allen (1970) highlighted the main limitation of deducing physical sedimentary processes from climbing-ripple co-sets: “On the cautionary note, all that can be deduced from the geometrical properties of climbing-ripple cross-lamination is the ratio of the sediment deposition rate to the bedload transport rate”. In other words, high angles of climbing-ripple co-sets may be formed by any aggradation rate, provided that the ripple migration rate is significantly lower than the aggradation rate. For example, simple trigonometry can be used to show that a high climbing angle of 20° can be achieved at a low aggradation rate of 0.001 mm s^{-1} by ripples that migrate at a low rate of 0.003 mm s^{-1}, or at a high aggradation rate of 0.1 mm s^{-1} and with a high ripple migrate rate of 0.3 mm s^{-1}. In very fine sand, these two ripple migration rates are associated with either low flow velocities close to the threshold of sediment motion (c. 0.25 m s^{-1}) or high flow velocities near the transition to washed-out ripples and upper-stage plane bed conditions (c. 0.60 m s^{-1}), respectively (Baas et al., 2000). It is therefore essential to use other physical sedimentological parameters, in addition to angle of climb, to estimate the aggradation rate from climbing-ripple co-sets, and from this the duration of deposition represented by these co-sets. The main text of the present paper provides qualitative support for high aggradation rates. Herein, a complimentary more quantitative approach is outlined. It is assumed that the orientation of the climbing-ripple co-set is parallel to the paleoflow direction, as supported by a maximum foreset slope angle of 27°, which is close to the angle of repose for loose sand. This high slope angle also suggests that post-depositional compaction did not significantly influence the ripple height.

As discussed in the main text, the climbing-ripple set is divided into three sectors, representing a progressive change from turbulent flow (Sector 1), through turbulence-enhanced transitional flow and lower transitional plug flow (Sector 2), to upper transitional plug flow and quasi-laminar plug flow (Sector 3), with the transitional flow terms sensu Baas et al. (2009). Our quantitative assessment of aggradation rates and duration of deposition for each of these three sectors in the climbing-ripple set is given below, before estimating the total time needed to form the climbing-ripple set.

Sector 1 – Sandy current ripples formed by turbulent flow

Ripple development

Sector 1 of the climbing-ripple set has an average climbing angle of 19.7°, with a ripple migration distance of 43.6 mm and an aggradation height of 15.6 mm. These sandy ripples grew in height from 8.5 mm to 12.9 mm between the base and top of Sector 1. The final height of 12.9 mm is below 14.9 mm, which, for the 0.124 mm sand observed herein, is the height at which the ripples are in equilibrium with the flow conditions, based on the ripple size predictor of Baas (1993):

$$H_e = 3.4\ log_{10}(D_{50}) + 18 \qquad \text{(S1)}$$

where H_e is the equilibrium height in millimeters and D_{50} is the median grain size in millimeters. It is therefore inferred that in Sector 1 the ripples did not reach equilibrium and evolved between non-equilibrium heights of 8.5 mm and 12.9 mm. Current ripples in 0.124 mm sand form at flow velocities between c. 0.25 m s^{-1} and 0.80 m s^{-1} in flow depths of more than 0.25 m (Southard & Boguchwal, 1990; their figure 3). Following the current ripple development model of Baas (1993) and interpolating between 0.095 mm sand (Baas, 1994) and 0.238 mm sand (Baas, 1999), ripples at these velocities need c. 2253 hours at 0.25 m s^{-1} and c. 6.6 minutes at 0.80 m s^{-1} to reach the observed final height of 12.9

mm. This large range in duration of deposition can be constrained in different ways, as detailed in the following sub-sections.

Migration rate

The ripple migration rates for flow velocities between 0.25 m s^{-1} and 0.80 m s^{-1}, after conversion from Shields parameter to flow velocity and interpolation between 0.095 mm and 0.238 mm sand (Baas et al., 2000; their figure 1) range from 0.0037 mm s^{-1} to 2.18 mm s^{-1}, respectively. These migration rates, at the migration distance of 43.6 mm in Sector 1, result in durations of deposition of between 0.3 minutes and 196 minutes. Hence, the time needed to deposit Sector 1 of the climbing-ripple set is reduced to 6.6 - 196 minutes.

Transition from angular to sigmoidal foresets

Ashley et al. (1982) found experimentally that the foreset laminae of sandy climbing ripples change from angular to sigmoidal, as the aggradation rate is increased from 0.0067 mm s^{-1} to 0.015 mm s^{-1}. Since the cross-laminae in the climbing-ripple set are clearly sigmoidal (Fig. 1B), this approach can be used to estimate the duration of deposition. At the aggradation height of 15.6 mm in the climbing-ripple set under consideration herein, these aggradation rates translate into durations of deposition of 38.8 minutes and 17.3 minutes, respectively. This suggests that this set was formed within 38.8 minutes, thus further constraining the duration of deposition to 6.6 - 38.8 minutes.

Turbidite duration estimation (TDURE) model

Baas et al. (2000) and Baas (2004) used the TDURE model to calculate the duration of deposition of sediment from the thickness of Ta, Tb and Tc divisions, and the height and angle of climb of climbing ripples in Bouma-type turbidites (Bouma, 1962). For the present case, TDURE yields a duration of deposition for Sector 1 of 1.2 minutes. However, this duration is a crude estimate, because TDURE assumes that: (i) the ripples start to form on an upper-stage plane bed; and (ii) the top of the climbing-ripple co-set represents slow flow at the threshold of sediment motion. Both of these conditions need not be representative of the sample studied herein. The base of the climbing ripple set may have formed at any velocity in the current ripple stability regime; lower initial velocities would increase the predicted duration of deposition of Sector 1. Moreover, the top of the set was probably formed at a velocity significantly above the threshold of sediment motion (*c.* 0.25 m s^{-1} for 0.124 mm sand), given that the ripples kept climbing steeply into Sector 2, which would decrease the predicted duration of deposition of Sector 1. Yet, the short duration predicted by TDURE, together with the above constraint of the duration of deposition to 6.6 - 38.8 minutes, renders it unlikely that the duration of deposition was longer than several tens of minutes.

Flow deceleration: the clay flow phase diagram

Given the muddy character of the deposits below, above and within the climbing-ripple co-set, we assume that the climbing ripples in Sector 1 were formed in a flow that carried cohesive clay. The velocity range at which current ripples form in 0.124 mm sand is linked to clay concentration through the clay flow phase diagram of Baas et al. (2009; Fig. S2). This diagram shows the stability regimes of turbulent, transitional and laminar clay flow as a function of flow velocity and suspended clay (kaolinite) concentration. Because the Sector 1 ripples formed in turbulent flow, the suspended clay concentration should have been below 4% (*i.e.* where 0.80 m s^{-1} crosses the boundary between turbulent flow [TF] and turbulence-enhanced transitional flow [TETF]), or at progressively lower maximum clay concentrations if the Sector 1 ripples formed below 0.80 m s^{-1}, since the TF-TETF boundary shifts to lower clay concentrations as the velocity decreases. The yellow, red and purple arrows in Fig. S2 show three possible paths for the flow that formed the climbing-ripple set. The yellow arrow presumes that the flow decelerates, but the suspended concentration is constant (or weakly decreasing or increasing) during deceleration. This scenario is unlikely to explain the formation of the climbing-ripple set for two principal reasons: (i) the flow would be incapable of reaching upper-transitional plug flow or quasi-laminar plug flow behavior required to form Sector 3 of the climbing-ripple set before the velocity becomes too low for ripple migration at 0.25 m s^{-1}; and (ii) a constant (or weakly decreasing or increasing) clay concentration is unlikely in waning flow and contrasts with the upward increase in clay content in the deposit. The red arrow represents a scenario in which the climbing-ripple set starts to form at a low velocity and then decelerates over a narrow range of velocities. This scenario requires a strong increase in clay concentration of almost two orders of magnitude to pass the various clay flow types needed to form all three sectors of the climbing-ripple set. This combination of weak flow waning and strong bulking of the flow with clay would be difficult to achieve without invoking specific external factors, such as tapping into an upstream clay source during development of the climbing-ripple co-set. A combination of deceleration over a wider range of velocity and a narrower range of clay concentration is a more plausible scenario (purple arrow in Fig. S2), because a large decrease in velocity is often associated hydrodynamically with increased fallout of clay from suspension and thus an increase in clay concentration above the ripple crest and in the ripple trough. This scenario thus also explains the vertical increase in clay content in the climbing-ripple set. Moreover, the clay concentration does not need to increase over two orders of magnitude, as the clay concentration of the flow that formed the first ripple in Sector 1 of the climbing-ripple set may have carried up to 4% clay. Since a high initial velocity in the ripple regime is required to achieve the strong flow waning in this scenario, this increases the likelihood that the ripples in Sector 1 migrated rapidly and therefore the climbing ripple was exposed to rapid aggradation to maintain the climbing angle. In turn, this suggests that the duration of deposition of these sandy ripples was shorter than estimated with the above methods for determining flow velocity and ripple migration rate, because migration rate increases exponentially with flow velocity (Baas et al., 2000). For example, the above estimate of 6.6 - 196 minutes, based on maximum and minimum ripple migration rate, is reduced to 6.6 - 31.0 minutes and 6.6 - 7.8 minutes, if the climbing-ripple set was formed at Sector-1 averaged velocities of 0.35 m s^{-1} and 0.45 m s^{-1}, respectively. These ranges are comparable to those inferred from the foreset laminae shape (Ashley et al., 1982) and the TDURE model (Baas, 2004) above.

Settling rate

Jobe et al. (2012) used the following relationship between aggradation rate and particle fall velocity under hindered settling conditions for the analysis of climbing-ripple co-sets:

$$w_{s,h} C_{susp} = U_{bed} C_{bed} \tag{S2}$$

where $w_{s,h}$ is the fall velocity corrected for hindered settling, C_{susp} is the concentration of sand or silt particles in the flow, U_{bed} is the bed aggradation rate, and $C_{bed} = 0.65$ is the concentration of the sand or silt particles in the bed, assuming a random packing density. Values for $w_{s,h}$ were calculated from the hindered settling relationship of Richardson & Zaki (1954):

$$w_{s,h} = w_s (1 - C_{susp})^{4.65} \tag{S3}$$

where w_s is the fall velocity of a single particle in clear water. The fall velocity for 0.124 mm sand particles in clear water is 0.012 m s^{-1} (Soulsby, 1997). Combining Equations S2 and S3 and using a realistic range of C_{susp}-values for turbulent sediment gravity flows of 0.5% to 4% (*cf.* Fig. S2) yields $0.088 < U_{bed} < 0.60$ mm s^{-1}. For Sector 1 of the climbing-ripple set, this converts into a duration of deposition of between 0.4 minutes and 3.0 minutes. However, the fall velocity used herein may be overestimated, because the very fine sand particles did not settle through quiescent water, and thus turbulence in the flow will have reduced the fall velocity, and the presence of up to 4% clay will have further reduced the fall velocity through enhanced hindered settling and increasing the water viscosity. However, even if this reduction had been an order of magnitude, the duration of deposition of Sector 1 would have increased to only 4.3 - 29.5 minutes, well within the range of durations calculated with the above methods.

Summary for Sector 1

Although no precise values for the duration of deposition for the sandy ripples in Sector 1 of the climbing-ripple set can be calculated, the combination of methods used herein implies that Sector 1 was formed rapidly, within time periods of minutes to several tens of minutes.

Sector 2 – Mixed sand–clay large ripples formed by turbulence-enhanced transitional flow and lower transitional plug flow

Sector 2 of the climbing-ripple set has an average angle of climb of 18.4°, with a ripple migration distance of 83.3 mm and an aggradation height of 27.7 mm. These heterolithic sand–clay ripples grew in height from 12.9 mm to 21.7 mm between the base and top of Sector 2. Two different approaches are taken herein to estimate the duration of deposition in the sub-sections below.

Comparison with experiments of Baas et al. (2011)

Large ripples in cohesive mixed sand–clay flows were described for the first time by Baas et al. (2011). The kinematic behavior of large ripples is more poorly known than that of the type of sandy ripples present in Sector 1, which have been studied for more than a century (*e.g.* Sorby 1859, 1908). Consequently, the duration of deposition of the large ripples in Sector 2 is more difficult to estimate than in Sector 1. Baas et al. (2011) described large ripples in heterolithic deposits of kaolinite clay and poorly sorted silty sand (median diameter: 0.084 mm). These large ripples formed at a mean flow velocity of 0.44 m s^{-1}, were up to 18 mm high and 203 mm long, and migrated at a rate that decreased from 0.236 mm s^{-1} to 0.133 mm s^{-1}, as suspended clay concentration was increased from 1.1% to 8.0%. These numerical values are of the same order of magnitude as those inferred to predict durations of deposition, for the climbing ripple set examined herein, from the clay flow phase diagram of Baas et al. (2009) (*e.g.* purple arrow in Fig. S2). Applying migration rates of 0.133 mm s^{-1} to 0.236 mm s^{-1} to the climbing-ripple set in Sector 2 yields durations of deposition of 10.4 minutes and 5.9 minutes, respectively. These durations should be considered approximate, because the mean velocity at which the large ripples formed may not have been close to 0.44 m s^{-1}. A higher and lower mean velocity for Sector 2 would decrease and increase the duration of deposition, respectively.

Bed sediment flux and ripple height

Interestingly, the bed sediment flux associated with ripple migration is nearly constant (0.9 - 1.1 mm^2 s^{-1}) over almost the entire range of suspended clay concentrations (0.2 - 6.9%) at which 'normal' current ripples and large ripples were the stable bedform phase in the experiments of Baas et al. (2011; their figure 15c). Because the bed sediment flux is dependent on the product of ripple migration rate and ripple height, and ripple migration rate decreased as clay concentration was increased in the experiments of Baas et al. (2011), the bed sediment flux was governed primarily by the ripple height. Hence, an increase in ripple height in steady flow should result in a proportional decrease in ripple migration rate. If it is assumed that this relationship is applicable to other flow velocities and sediment sizes, and taking the conservative estimate of the Sector 1 duration of deposition of 6.6 - 38.8 minutes, Sector 2 could have been deposited in 21.2 - 125 minutes. This increase in duration reflects the increase in ripple height from 12.9 mm in Sector 1 to 21.7 mm in Sector 2, and the larger aggradation distance of Sector 2. However, these calculations do not include the possible contribution to the migration rate of the large ripples by fallout from suspension of clay particles, which make up more than half of the foreset laminae in Sector 2 (Fig. 1A,B), and that are also thicker than the clay-rich laminae shown in Baas et al. (2011). Incorporating this extra downward flux is expected to reduce the duration of deposition of Sector 2, but a precise reduction cannot be calculated at present.

Summary for Sector 2

We conclude that the two methods used herein suggest that several minutes to several tens of minutes were required to form Sector 2 of the climbing-ripple set. The rapid aggradation rate in Sector 1 thus continued into Sector 2.

Sector 3 – Clay-rich ripples formed by upper transitional plug flow and quasi-laminar plug flow

Sector 3 of the climbing-ripple set has an average angle of climb of 44.2°, with a ripple migration distance of 22.2 mm and an aggradation height of 21.6 mm. The height of these clay-rich ripples decreases from 21.7 mm to 18.4 mm between the base and top of Sector 3. The duration of deposition of this section is estimated in two different ways detailed below.

Bed sediment flux and ripple height

As for the large ripples in Sector 2, a small amount of information is available from past work concerning the kinematics of clay-rich bedforms, which are interpreted to have formed by upper transitional plug flow and quasi-laminar plug flow in Sector 3 of the climbing-ripple set. Baas et al. (2011; their figure 11) measured the aggradation rate in the same rapidly decelerated kaolinite clay flows that formed the large ripples described above, but at higher suspended clay concentrations of 10.1% to 19.2%. In the first 15 minutes after flow deceleration, when the flow velocity was steady at 0.44 m s^{-1}, the mean aggradation rate ranged from 0.005 mm s^{-1} to 0.023 mm s^{-1}. Using these aggradation rates, the 21.6 mm thick Sector 3 is predicted to have been deposited in 15.5 - 69.0 minutes. However, the aggradation rate at a fixed suspended clay concentration is expected to vary with flow velocity.

Settling rate

The settling velocity of clay particles is highly dependent on flocculation, but, owing to the low salinity of the water in the caldera lake, the clay may have aggregated into microflocs (Eisma, 1986), rather than staying as single clay particles that are rare in nature (Schieber et al., 2007), or forming larger macroflocs that are common in more saline water. The diameter of microflocs was delimited by Mikkelsen et al. (2006) to 0.036 - 0.133 mm, and the settling velocity of such microflocs is *c.* 0.126 mm s^{-1} to 0.463 mm s^{-1} (Fig. S4), which corresponds well with the mean settling velocity of 0.34 mm s^{-1} for fresh-water flocs derived from eight major rivers (Lamb et al., 2020). These settling velocities were derived from the 'model' curve in Fig. S4, which denotes the relationship between the settling velocity for a single floc, w_s, and floc diameter, D_f (Mehta, 2013):

$$w_s = \frac{\alpha}{18\beta}\frac{(\rho_{s-}\rho_w)g}{\mu}D_p^{3-n_f}\frac{D_f^{n_f-1}}{1+0.15Re_f^{0.687}} \quad \text{(S4)}$$

where $\alpha = \beta = 1$ are particle shape factors, ρ_s is the density of the primary clay particle, ρ_w is the water density, μ is the dynamic viscosity, D_p is the diameter of the primary clay particle, n_f is the fractal dimension of the floc, taken herein as 2 (Fig. S4; Mehta, 2013), $Re_f = w_s D_f / \nu$ is the floc Reynolds number, and ν is the kinematic viscosity. Typical suspended clay concentrations for upper transitional plug flow and quasi-laminar plug flow within the expected range of flow velocities (Fig. S2) are between 5% and 10%, and thus well within the hindered settling regime. Using Equations S2 and S3, and following the same procedure as for the large ripples in Sector 2, estimated aggradation rates for the climbing ripples in Sector 3 are between 0.0077 mm s^{-1} and 0.044 mm s^{-1}, which is equivalent to durations of deposition of 8.2 - 47.0 minutes.

Summary for Sector 3

The two methods used herein to estimate the duration of deposition of the mud-rich climbing ripples in Sector 3 both yield time periods of tens of minutes.

Conclusion

Our quantitative analysis of the climbing-ripple sets studied in this paper shows that the sandy ripples in Sector 1 and the heterolithic mixed sand–clay large ripples in Sector 2 formed within minutes to tens of minutes. The generation of the mud-rich ripples in Sector 3 may have needed somewhat longer, *i.e.* of the order of ten of minutes. We conclude that the entire climbing-ripple set was thus deposited within several tens of minutes. Such a duration supports the notion that the climbing-ripple set records rapid transformation from turbulent via turbulent-enhanced to a turbulence-attenuated sediment gravity flow.

References

Allen, J. R. L., 1963, Asymmetrical ripple marks and the origin of water-laid cosets of cross-strata: Liverpool Manchester Geological Journal, v. 3, p. 187-236.

Allen, J. R. L., 1970, A quantitative model of climbing ripples and their cross-laminated deposits: Sedimentology, v. 14, p. 5-26.

Ashley, G. M., Southard, J. B., and Boothroyd, J. C., 1982, Deposition of climbing-ripple beds: a flume simulation: Sedimentology, v. 29, p. 67-79.

Baas, J. H., 1993, Dimensional analysis of current ripples in recent and ancient depositional environments: Geologica Ultraiectina, v. 106, p. 199.

Baas, J. H., 1994, A flume study on the development and equilibrium morphology of small-scale bedforms in very fine sand: Sedimentology, v. 41, p. 185-209.

Baas, J. H., 1999, An empirical model for the development and equilibrium morphology of current ripples in fine sand: Sedimentology, v. 46, p. 123-138.

Baas, J. H., 2004, Conditions for formation of massive turbiditic sandstones by primary depositional processes: Sedimentary geology, v. 166, p. 293-310.

Baas, J. H., van Dam, R. L., and Storms, J. E. A., 2000, Duration of deposition from decelerating high-density turbidity currents: Sedimentary Geology, v. 136, p. 71-88.

Baas, J. H., Best, J. L., Peakall, J., and Wang, M., 2009, A phase diagram for turbulent, transitional, and laminar clay suspension flows: Journal of Sedimentary Research, v. 79, p. 162-183.

Baas, J. H., Best, J. L., and Peakall, J., 2011, Depositional processes, bedform development and hybrid flows in rapidly decelerated cohesive (mud-sand) sediment flows: Sedimentology, v. 58, p. 1953-1987.

Baas, J. H., Best, J. L., and Peakall, J., 2016, Comparing the transitional behaviour of kaolinite and bentonite suspension flows: Earth Surface Processes and Landforms, v. 41, p. 1911-1921.

Banerjee, I. 1977, Experimental study on the effect of deceleration on the vertical sequence of sedimentary structures in silty sediments: Journal of Sedimentary Research, v. 47, p. 771-783.

Bouma, A. H., 1962, Sedimentology of Some Flysch Deposits: A Graphic Approach to Facies Interpretation: Elsevier, Amsterdam/New York, 168 p.

Eisma, D., 1986, Flocculation and de-flocculation of suspended matter in estuaries: Netherlands Journal of Sea Research, v. 20, p. 183-199.

Jobe, Z. R., Lowe, D. R., and Morris, W. R., 2012, Climbing-ripple successions in turbidite systems: depositional environments, sedimentation rates and accumulation times: Sedimentology, v. 59, p. 867-898.

Jopling, A. V., and Walker, R. G., 1968, Morphology and origin of ripple-drift cross-lamination, with examples from the Pleistocene of Massachusetts: Journal of Sedimentary Petrology, v. 38, p. 971-984.

Lamb, M. P., de Leeuw, J., Fischer, W. W., Moodie, A. J., Venditti, J. G., Nittrouer, J. A., Haught, D. and Parker, G., 2020, Mud in rivers transported as flocculated and suspended bed material: Nature Geoscience, doi.org/10.1038/s41561-020-0602-5.

Mehta, A. J., 2013, An Introduction To Hydraulics Of Fine Sediment Transport: Advanced Series On Ocean Engineering, World Scientific Publishing Company, v. 38, 1060 p.

Mikkelsen, O. A., Hill, P. S. and Milligan, T. G., 2006, Single-grain, microfloc and macrofloc volume variations observed with a LISST-100 and a digital floc camera: Journal of Sea Research, v. 55, p. 87-102.

Reineck, H. E., 1961, Sedimentbewegungen an Kleinrippeln im Watt: Senckenbergiana Lethaea, v. 42, p. 51-67.

Richardson, J. F., and Zaki, W. N., 1954, Sedimentation and fluidisation: Part I: Transactions of the Institution of Chemical Engineers, v. 32, p. 35-53.

Schieber, J., Southard, J. and Thaisen, K., 2007, Accretion of mudstone beds from migrating floccule ripples: Science, v. 318, p. 1760-1763.

Sorby, H. C., 1859, On the structures produced by the currents present during the deposition of stratified rocks: The Geologist, v. 2, p. 137-147.

Sorby, H. C., 1908, On the application of quantitative methods to the study of the structure and history of rocks: Quarterly Journal of the Geological Society of London, v. 64, p. 171-233.

Soulsby, R., 1997, Dynamics of Marine Sands: A Manual for Practical Applications: Thomas Telford Publications, London, 272 p.

Southard, J. B., and Boguchwal, L. A., 1990, Bed configurations in steady unidirectional water flows. Part 2. Synthesis of flume data: Journal of Sedimentary Petrology, v. 60, p. 658-679.

Środoń, J. 1974, An interpretation of clipping-ripple cross-lamination, Annales de la Société Géologique de Pologne: v. 44, p. 449-473.

Walker, R. G., 1963, Distinctive types of ripple-drift cross-lamination: Sedimentology, v. 2, p. 173-188.

Figure captions

Fig. S1. Horizontal position of the ripple brinkpoint vs ripple height for two climbing ripple sets. Blue dots denote the climbing ripple set shown in Fig. 1. The open circles denote the downstream climbing ripple set (right-hand side of Fig. 1A).

Fig. S2. Clay flow phase diagram, showing the relationship between suspended clay concentration, for kaolinite clay, and depth-averaged flow velocity (modified after Baas et al., 2009). Turbulent, transitional and laminar flow types are highlighted by orange shadings. The blue dashed lines indicate boundary velocities between which current ripples form in very fine sand (Baas, 1993). The blue dot denotes the maximum kaolinite clay concentration at which current ripples can be generated in turbulent flow. Since kaolinite is a weakly cohesive clay mineral, this maximum concentration will be lower for other clay minerals, such as illite and bentonite (Baas et al., 2016). The gray dashed lines signify flow velocities of 0.35 m s^{-1} and 0.45 m s^{-1} used in the text. The yellow, red, and purple arrows indicate different flow paths for the flow that generated the climbing-ripple set, discussed in the text.

Fig. S3. Original (top) and interpreted (bottom) close-up photograph of backflow ripples on the lower slipface of the climbing ripples. See Fig. 1B for location.

Fig. S4. Functional relationship between the settling velocity, w_s, and diameter of mud flocs, D_f (modified after Mehta, 2013). The gray area delimits the field data used to define the black curves (see Equation S4). The three curves use different fractal dimensions, n_f. The present study uses $n_f = 2.0$. The blue dashed lines denote the limits of the size of microflocs in fresh water, according to Mikkelsen et al. (2006).

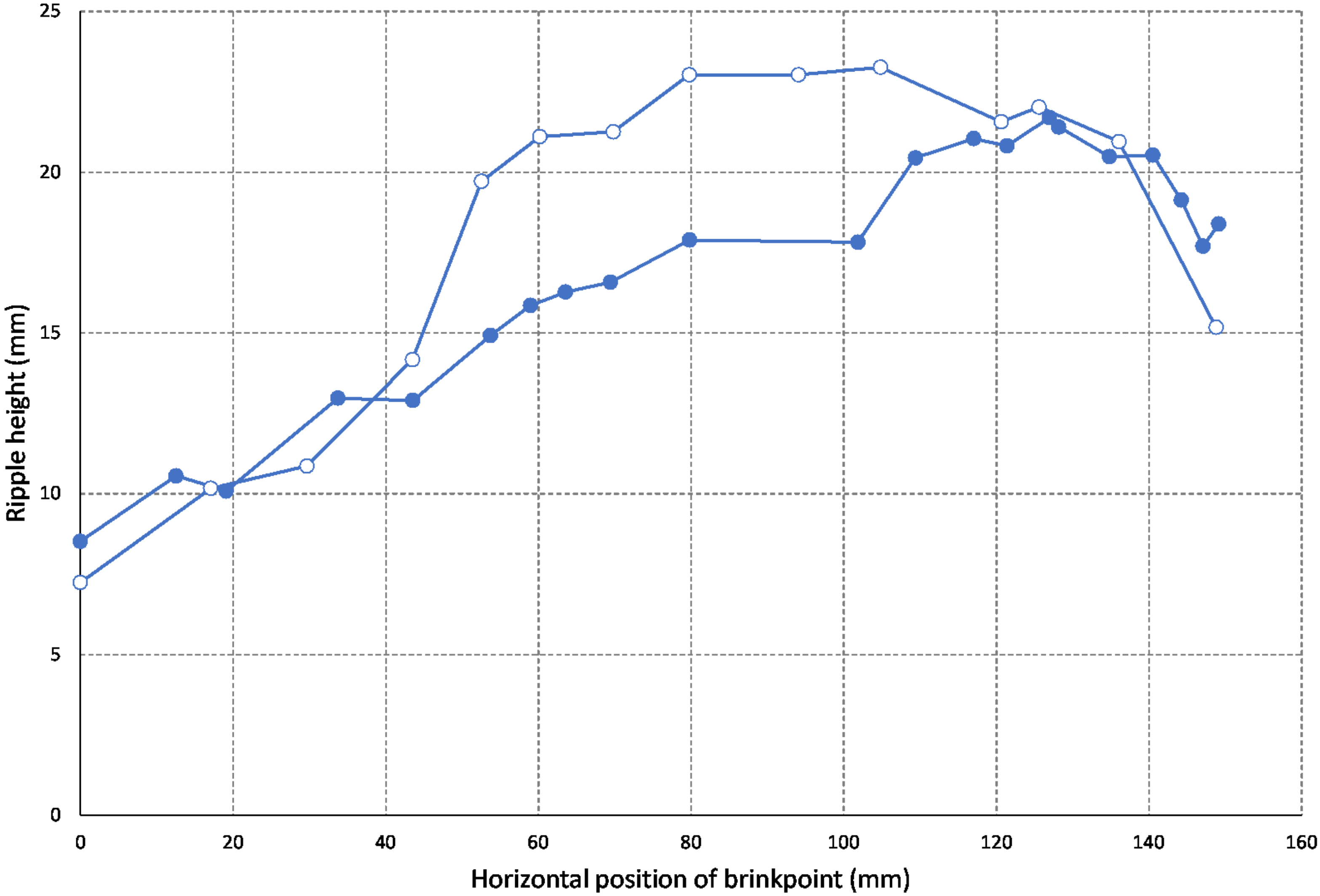
25
20
15
10
5
0
Ripple height (mm)
0
20
40
60
80
100
120
140
160
Horizontal position of brinkpoint (mm)

Data Repository File DR3

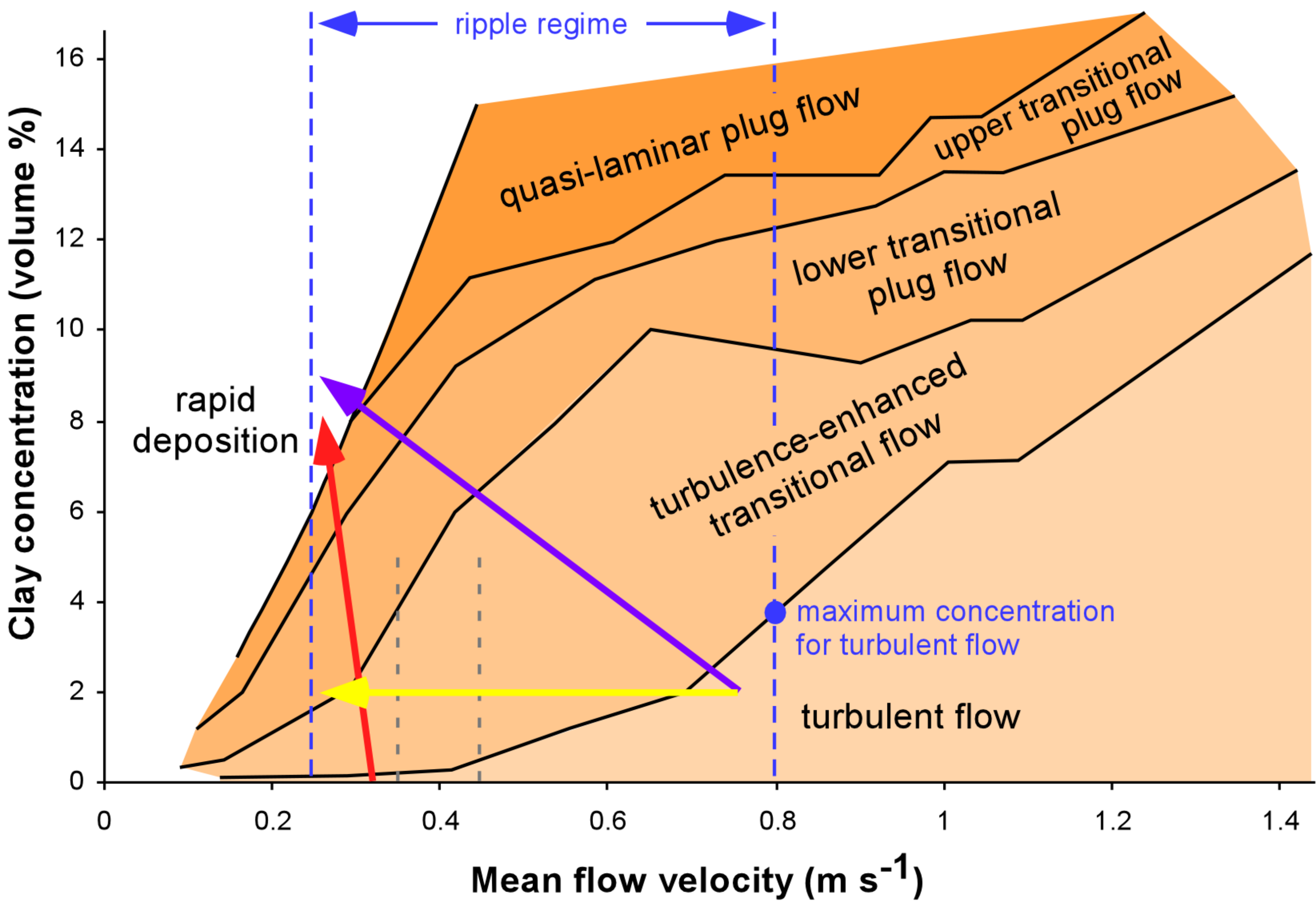

Data Repository File DR3

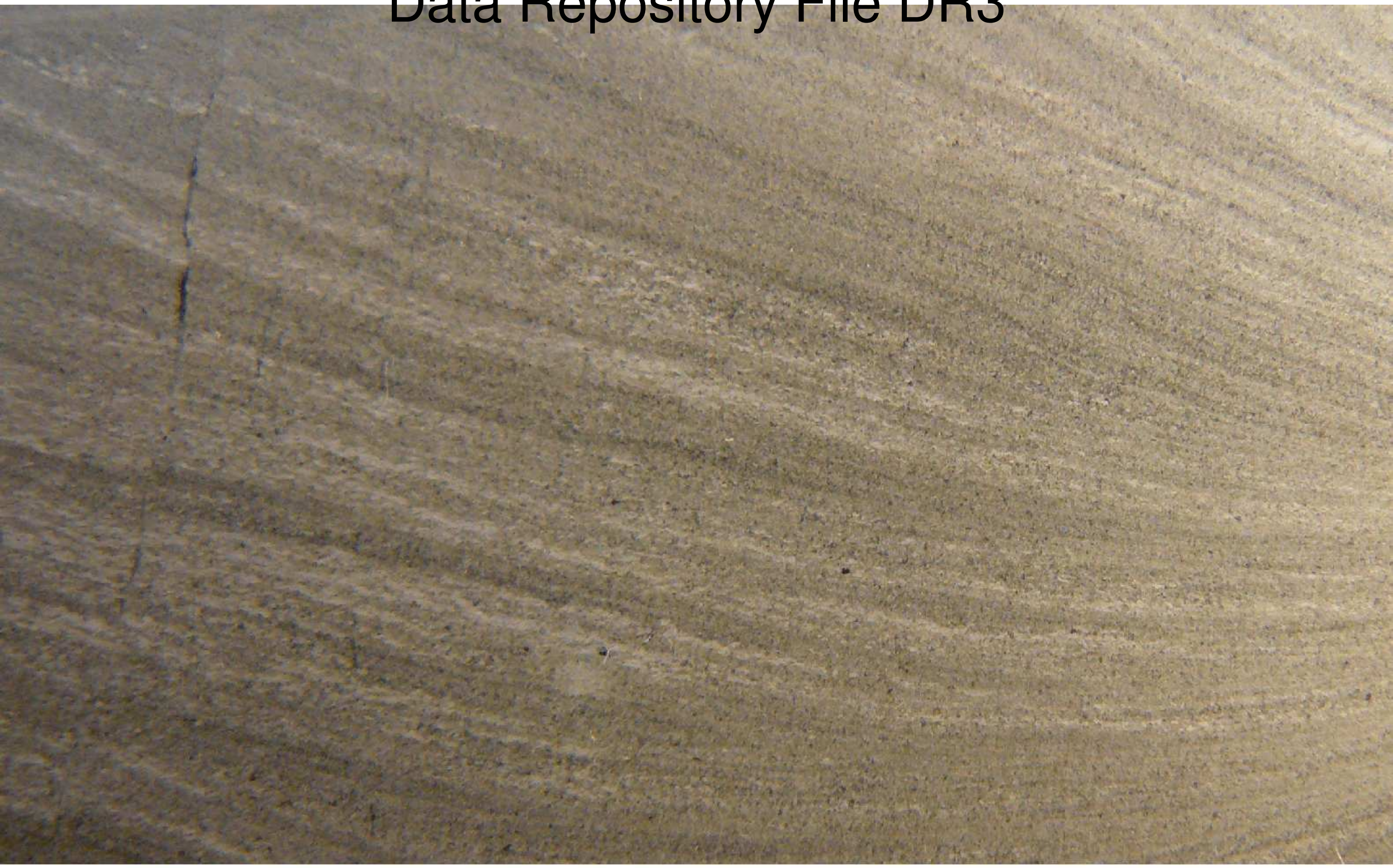

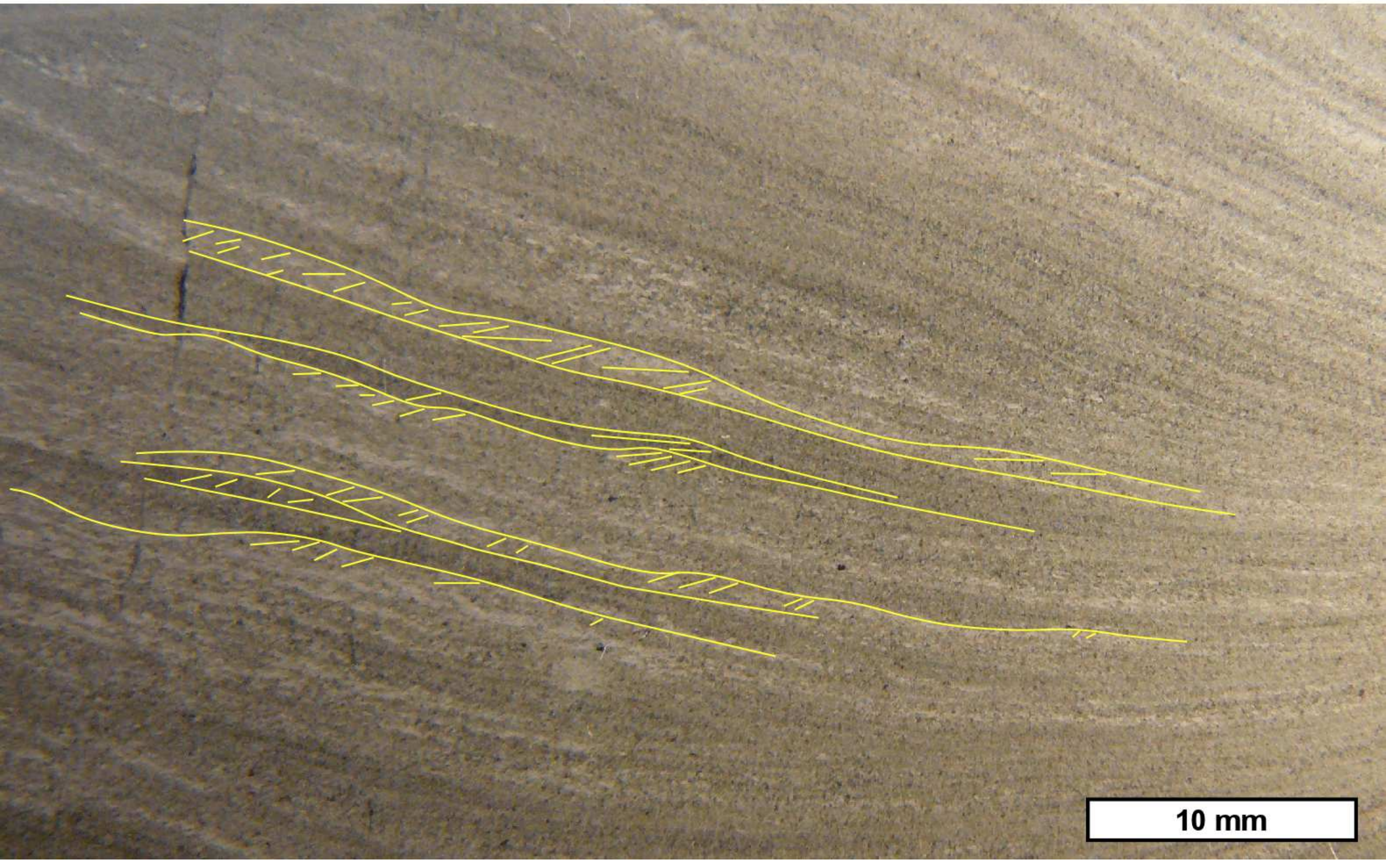

Data Repository File DR3